

## Inelastic neutron scattering in single-crystal YbInCu<sub>4</sub>

J. M. Lawrence

*University of California, Irvine, California 92697*

S. M. Shapiro

*Brookhaven National Laboratory, Upton, New York 11973*

J. L. Sarrao and Z. Fisk

*National High Magnetic Field Laboratory, Florida State University, Tallahassee, Florida 32306*

(Received 2 December 1996)

We have measured the momentum and energy dependence of the spin fluctuations in the low-temperature mixed-valent state and the high-temperature integral-valent state of YbInCu<sub>4</sub>, using flux-grown single crystals and a triple axis spectrometer. The magnetic scattering can be fit with a Lorentzian power spectrum, with positions and halfwidths equal  $E_0^+ = 2.3$  meV and  $\Gamma^+ = 1.8$  meV in the high-temperature state at 50 K and  $E_0^- = 40.2$  meV and  $\Gamma^- = 12.3$  meV in the low-temperature state at 20 K. Within the experimental uncertainties, the line shape as a function of energy transfer (i.e., the power spectrum) does not depend on momentum transfer  $Q$ . The static susceptibility  $\chi(Q)$  is no more than 10% larger at the zone boundary than at zone center for the [1,0,0] direction. The results compare reasonably well to the predictions of the Anderson impurity model and to earlier measurements on polycrystalline samples. [S0163-1829(97)04121-0]

### INTRODUCTION

The compound YbInCu<sub>4</sub> exhibits a first-order phase transition at  $T_s = 40$  K (Refs. 1 and 2) that is similar to the  $\alpha$ - $\gamma$  transition in cerium metal.<sup>3</sup> At high temperature the material is nearly trivalent, with localized paramagnetic  $4f$  electrons; at low temperature, it becomes a mixed-valent Pauli paramagnet. The density changes by 0.5% at the transition, but conventional x-ray diffraction studies suggest that there is no change in the cubic (*C15b*) structure. Recently, we have found that large single crystals can be grown by precipitation from liquid InCu flux.<sup>4</sup> Structural refinement, using neutron-diffraction data from a spallation neutron source, shows that these crystals are more highly ordered than the polycrystals used in past studies and confirms that the ground-state structure is *C15b*.<sup>5</sup> Given the high quality of these crystals, and given that YbInCu<sub>4</sub> provides an excellent example for studying the physics of mixed-valence and of first-order valence transitions, we have begun a thorough characterization of this and related compounds.

The focus of the present paper is inelastic-magnetic neutron scattering. Our main goal is to use the single crystal to test for any  $Q$  dependence of the dynamical susceptibility. Existing work<sup>6</sup> on polycrystals, utilizing time-of-flight measurements with maximum energy transfer of 50 meV, showed that in the low-temperature mixed-valent state the scattering exhibits a broad maximum centered near 40 meV, while at high temperature, a scattering maximum occurs near 3 meV. The former energy represents the large characteristic energy of the mixed-valent state; the high-temperature scattering was interpreted as arising from crystal-field levels. Herein we report a study of the inelastic scattering from a single crystal, for which we used a triple-axis spectrometer and extended the study to higher-energy transfer (65 meV). Most past studies (e.g., Ref. 7) of inelastic scattering in

mixed-valent compounds utilized polycrystals, and hence were not designed to study the full  $Q$  (momentum) dependence of the scattering. Use of a single crystal enables us to test very general ideas about mixed-valent compounds, in particular that the scattering is from highly localized spin fluctuations, with very little  $Q$  dependence and with nearly Lorentzian line shape.

### EXPERIMENTAL DETAILS

The samples were high-quality single crystals grown by precipitation from InCu flux, as described earlier.<sup>4</sup> The crystal was faceted, of irregular shape, and of approximate volume  $0.5 \text{ cm}^3$  with a uniform mosaic of order  $0.3^\circ$ . The magnetic susceptibility of a crystal of YbInCu<sub>4</sub> taken from the same growth batch and measured in a superconducting quantum interference device (SQUID) magnetometer is shown in Fig. 1(a). The absence of a low-temperature "Curie tail," and the fact that the transition at 40 K is very sharp, attests to the quality of these crystals. The sample was oriented so that the [011] direction was vertical and the [100] and [011] directions were in the scattering plane. It was mounted in a closed-cycle He refrigerator, and mounted on the H8 triple-axis spectrometer at the High-Flux-Beam reactor at Brookhaven National Laboratory. For smaller energy transfer, we operated with a fixed final-energy  $E_f = 14.7$  meV, a collimation of  $40'-40'-80'-80'$ , and a pyrolytic graphite (PG) filter after the sample; the resolution as measured by the full-width at half maximum (FWHM) of the elastic line was of order 1–1.5 meV, depending on momentum transfer. To determine the temperature dependence of the lattice constant we measured the (2,0,0) reflection and fit it to a Gaussian line shape to determine the peak position in reciprocal space; for this we used a collimation of  $20'-20'-20'-20'$ . For larger energy transfer we utilized a fixed final energy  $E_f = 30.5$

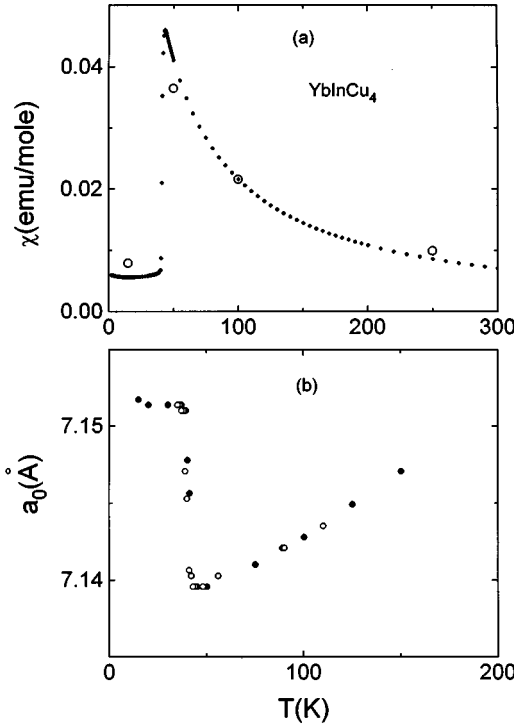


FIG. 1. (a) The dc susceptibility of  $\text{YbInCu}_4$ , measured in a SQUID magnetometer. The open circles give the static susceptibility deduced from the neutron scattering measurements (Figs. 3 and 4); these are scaled to equal the dc susceptibility at 100 K. (b) The lattice constant of  $\text{YbInCu}_4$  vs temperature, deduced from the temperature dependence of the position in  $Q$  of the (2,0,0) reflection.

meV and a collimation of  $40'-40'-40'-80'$ , again with a PG filter; here, the elastic line showed a FWHM of 3–3.5 meV. Most studies were performed at fixed momentum transfer; the values of  $Q$  given in the figures are expressed in units of  $2\pi/a_0$ . Scattering intensities in Figs. 2–7 are given for fixed monitor count (stated in the ordinate label) of incident neutrons. The absorption length of  $\text{YbInCu}_4$  at the wavelengths used in these experiments is 1 cm or more, comparable to or somewhat larger than the sample dimensions. From studies of how the absorption changed with sample angle we estimate that the effect of absorption on the magnetic line shapes reported below is less than 10%.

## RESULTS AND ANALYSIS

The lattice constant of  $\text{YbInCu}_4$  as a function of temperature is shown in Fig. 1(b). The data for  $T \leq 38$  K and  $T \geq 42$  K reproduce on warming (closed circles) and cooling (open circles); the two-phase region extends over 3–4 K and is centered at  $T_s = 40$  K. The lattice constant shows a discontinuity at the transition of 0.165%, so that the discontinuity in density is 0.5%.

Figure 2(a) shows the scattering in the low- and high-temperature phases for energy transfer  $E \leq 10$  meV and at a small momentum transfer [ $Q = (1.5, 0, 0)$ ] for which the scattering should be primarily magnetic. At 50 K ( $T > T_s$ ) in addition to the elastic peak centered at  $E = 0$  the scattering shows a peak at  $E \approx 2.5$  meV; on transforming to the low-temperature state, this peak disappears, and only background

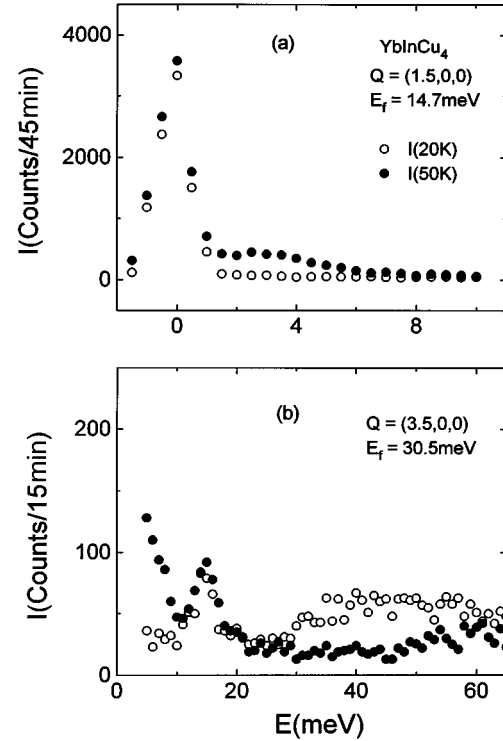


FIG. 2. Scattering intensity vs energy transfer  $E$  for  $\text{YbInCu}_4$  in the low-temperature state (open circles) and in the high-temperature state (closed circles). In (a) the data were collected at fixed final energy  $E_f = 14.7$  meV and for momentum transfer  $Q = (1.5, 0, 0)$  and the intensity is for fixed monitor count of  $45 \times 10^6$ ; in (b),  $E_f = 30.5$  meV and  $Q = (3.5, 0, 0)$  and the fixed monitor count is  $15 \times 10^6$ . (Throughout the paper,  $Q$  is given in units of  $2\pi/a_0$  and intensities are given for fixed monitor count.)

scattering is observed. Figure 2(b) shows the scattering at lower resolution, and for larger energy transfer. Here the momentum transfer [ $Q = (3.5, 0, 0)$ ] is such that a phonon peak is observed at  $E \approx 15$  meV at both 20 and 50 K. The inelastic scattering observed at 50 K for energy transfer  $E < 10$  meV is again observed to disappear at low temperature, being replaced by a broad feature centered near 40 meV. These results are similar to those observed earlier<sup>6</sup> in polycrystalline samples.

The observed scattering  $I_{\text{obs}}$  is a sum of the magnetic scattering  $I_{\text{mag}}$ , phonon scattering, background and multiple scattering, and elastic scattering near  $E = 0$ . However, only the magnetic scattering is expected to change at the first-order phase transition which occurs at  $T_s = 40$  K. Furthermore, for the small momentum transfer used for the higher resolution study [Fig. 2(a)] the phonon scattering should be small; and for the lower resolution study [Fig. 2(b)] the phonon peak at  $E = 15$  meV is well defined, and does not change significantly when the temperature increases from 20 to 50 K. Hence, by subtracting the low-temperature data from the high-temperature data we should to a good approximation eliminate all but the magnetic terms:

$$I_{\text{mag}}(E; Q; T^+) - I_{\text{mag}}(E; Q; T^-) \approx I_{\text{obs}}(E; Q; T^+) - I_{\text{obs}}(E; Q; T^-), \quad (1)$$

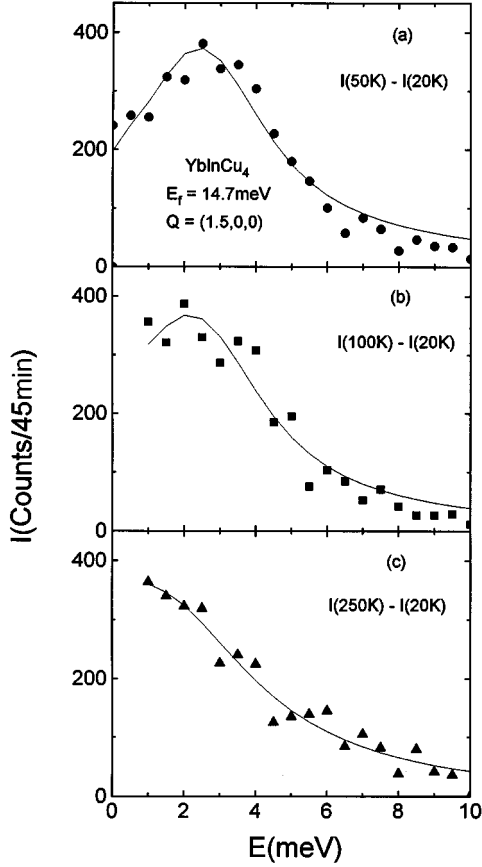


FIG. 3. The scattering intensity vs energy transfer in the high-temperature state for three temperatures (50, 100, and 250 K); the low-temperature data are treated as background and subtracted off, to give the magnetic scattering. The final energy is 14.7 meV and the momentum transfer is  $Q=(1.5,0,0)$ . The solid lines correspond to least squares fits to a Lorentzian power spectrum [Eqs. (1)–(3)] centered at  $E_0$  and with a width (HWHM)  $\Gamma$ . The fits give the following values: at 50 K,  $E_0^+ = 2.3$  meV and  $\Gamma^+ = 1.8$  meV; at 100 K,  $E_0^+ = 2.2$  meV and  $\Gamma^+ = 1.9$  meV, and at 250 K,  $E_0^+ = 1.4$  meV and  $\Gamma^+ = 2.9$  meV. (In these fits the values for the low-temperature state were fixed at  $E_0^- = 40$  meV and  $\Gamma^- = 12$  meV.) The fit values for the Lorentzian amplitudes are plotted in Fig. 1(a) as open circles, scaled to the dc susceptibility at 100 K.

where  $T^+ > T_s$  and  $T^- < T_s$ . We then assume that the magnetic scattering intensity at any temperature obeys the following relation:

$$I_{\text{mag}}(E; Q; T) = A \chi(Q) [n(E; T) + 1] f^2(Q) E P(E; T), \quad (2)$$

where  $A$  is an overall scale factor,  $\chi(Q)$  is the static susceptibility,  $[n(E; T) + 1]$  is the detailed balance factor, and  $f^2(Q)$  is the Yb  $4f$  form factor. For the normalized power spectrum we assume the form

$$P(E; T) = (\Gamma/2\pi) \{ \frac{1}{[E - E_0]^2 + \Gamma^2} + \frac{1}{[E + E_0]^2 + \Gamma^2} \}; \quad (3)$$

this is a commonly used<sup>8</sup> functional form to analyze the inelastic scattering of mixed-valent compounds. In the limit  $Q \rightarrow 0$  the static susceptibility  $\chi(Q)$  should vary with  $T$  proportional to the dc susceptibility  $\chi_{\text{dc}}(T)$ ; the inelastic peak

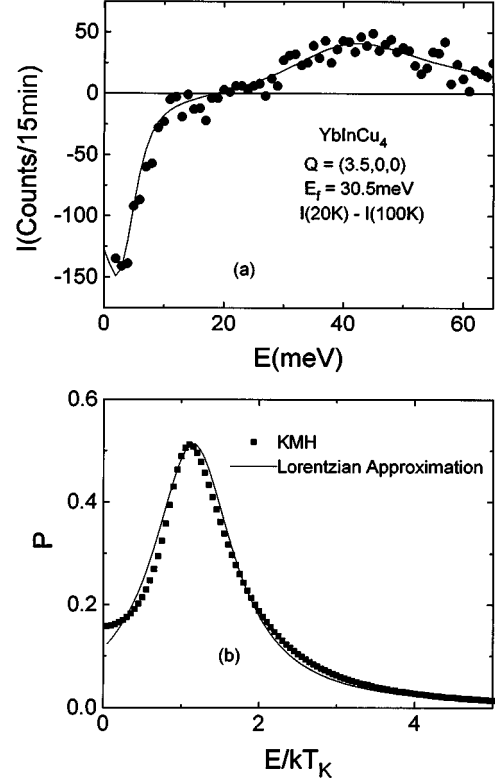


FIG. 4. (a) The difference between the scattering intensity in the low-temperature (20 K) and high-temperature (100 K) states. The final energy is 30.5 meV and the momentum transfer is  $(3.5, 0, 0)$ . The solid line corresponds to a least-squares fit to Eqs. (1)–(3) where the parameters for the high-temperature state are fixed at  $E_0^+ = 2.2$  meV and  $\Gamma^+ = 1.9$  meV; for the low-temperature state they are  $E_0^- = 40.2$  meV and  $\Gamma^- = 12.3$  meV. (b) The normalized power spectrum  $P(E)$  predicted by Kuramoto and Müller-Hartmann (KMH) (Ref. 14) for an Anderson impurity (solid symbols) plotted in units of the Kondo temperature. The solid curve demonstrates that a Lorentzian gives a good approximation to the predicted  $P(E)$ .

position  $E_0$  and the linewidth  $\Gamma$  have different values in the low- and high-temperature phases. As discussed below, the degree to which these three parameters depend on  $Q$  is a measure of the spatial correlation of the spin fluctuations.

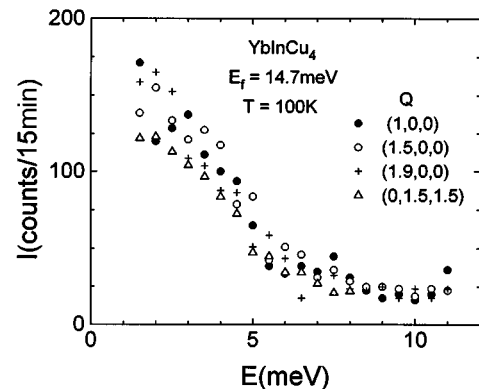


FIG. 5. The scattering intensity vs energy transfer in the high-temperature state (100 K) for several values of momentum transfer  $Q$  and for fixed final energy 14.7 meV. The scattering is essentially independent of  $Q$ .

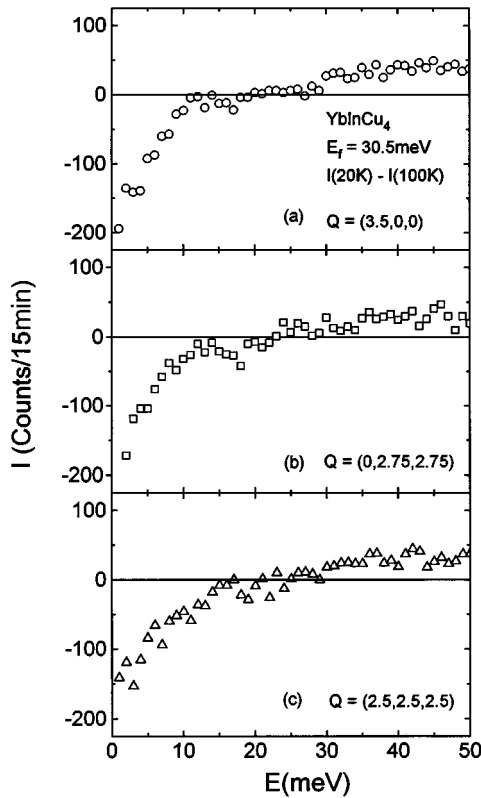


FIG. 6. The difference between the scattering intensity in the low-temperature state (20 K) and the high-temperature state (100 K) for momentum transfer  $Q$  at three different locations in the Brillouin zone. The final energy is fixed at 30.5 meV. The scattering is nearly independent of  $Q$ .

In Fig. 3 we present fits to the low-energy transfer data obtained at fixed final energy  $E_f = 14.7$  meV; in Fig. 4 we fit the data for  $E_f = 30.5$  meV. The solid symbols in Fig. 3 represent  $I_{\text{obs}}(T^+) - I_{\text{obs}}(T^-)$  where  $T^- = 20$  K and  $T^+ = 50, 100, \text{ and } 250$  K. [In Fig. 4 we plot  $I_{\text{obs}}(T^-) - I_{\text{obs}}(T^+)$ .] The lines represent least-squares fits for  $I_{\text{mag}}(T^+) - I_{\text{mag}}(T^-)$  based on Eqs. (2) and (3); we have convoluted Eq. (2) with a Gaussian to account for the instrumental resolution and the known variation of the spectrometer resolution with  $E_f$ ,  $Q$ , and  $E$ . The fits give the following values: at 20 K,  $E_0^- = 40.2$  meV and  $\Gamma^- = 12.3$  meV; at 50 K,  $E_0^+ = 2.3$  meV and  $\Gamma^+ = 1.8$  meV; at 100 K,  $E_0^+ = 2.2$  meV and  $\Gamma^+ = 1.9$  meV; and at 250 K,  $E_0^+ = 1.4$  meV and  $\Gamma^+ = 2.9$  meV. (The  $+/-$  superscripts refer to the high- and low-temperature phases.) The other parameters of the fit are the values of  $A\chi(Q)$  at the four temperatures 20, 50, 100, and 250 K; these are plotted in Fig. 1(a), where the values have been scaled so that  $\chi(Q) = \chi_{\text{dc}}$  at 100 K; the values of  $\chi(Q)$  clearly vary proportionally to the dc susceptibility. Given the statistics, we do not intend to exaggerate the degree to which Eqs. (2) and (3) fit the data; nevertheless, it is clear that the proposed Lorentzian power spectrum gives an adequate representation of the data and allows for extraction of meaningful values of the peak positions and linewidths in the low- and high-temperature phases.

We next turn to the  $Q$  dependence of the scattering. In

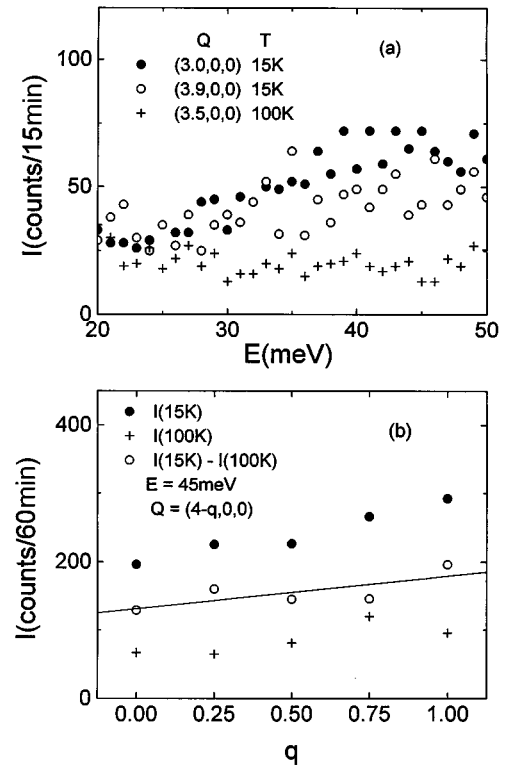


FIG. 7. (a) The scattering intensity vs energy transfer in the low-temperature state near zone center [ $Q = 3.9, 0, 0$ ] and at the zone boundary [ $Q = 3.0, 0, 0$ ] for the  $[1, 0, 0]$  direction; the scattering at 100 K is given to indicate the nonmagnetic background. (b) The scattering intensity at fixed energy transfer  $E = 45$  meV (corresponding to the peak intensity in part a) vs  $q$  where the momentum transfer is  $Q = (4 - q, 0, 0)$  in units of  $2\pi/a_0$ . The solid circles give the scattering in the low-temperature state; the crosses give the high-temperature scattering (representing the background), and the open circles give the magnetic scattering, taken as the difference between the low- and high-temperature scattering. The solid line is a least-square fit for the  $Q$  dependence of the magnetic scattering. (The final energy is fixed at 30.5 meV in this plot.)

Fig. 5 we show the observed scattering in the high-temperature state for four different  $Q$  in two different directions in reciprocal space ( $[1, 0, 0]$  and  $[0, 1, 1]$ ); for these  $Q$  and the given range of energy transfer, the observed scattering is dominated by the magnetic scattering. Minor variations in the scattering can be accounted for by the decrease of the form factor with increasing  $Q$ , the uncertainty due to absorption effects, and statistical uncertainty. Apart from this, the magnetic scattering in the high-temperature state is independent of  $Q$ , both in intensity and in its energy dependence.

In Fig. 6 we exhibit the magnetic scattering  $I_{\text{mag}}(T^-) - I_{\text{mag}}(T^+)$  found by application of Eq. (1) (with opposite sign), and as determined at lower resolution over a broader range of energy transfer, for three directions in the Brillouin zone. We note that the  $(3.5, 0, 0)$  point is halfway between the zone center and zone boundary along  $[1, 0, 0]$ ; the  $(2.5, 2.5, 2.5)$  point is at the  $[1, 1, 1]$  zone boundary and the  $(0, 2.75, 2.75)$  point lies at the  $[0, 1, 1]$  zone boundary. In this plot, the broad peak near 40 meV is due to the low-temperature magnetic scattering, while the negative peak at

low energy is due to the high-temperature scattering. It is clear that the scattering is very similar at all three  $Q$ . There is a slight decrease in intensity for  $Q=(2.5,2.5,2.5)$ , which can be accounted for by the decrease in magnetic form factor at this  $Q$ ; otherwise, we again assert that, within the uncertainties due to absorption effects and the counting statistics, the scattering is independent of  $Q$ , both in its energy dependence and its intensity.

To examine this more closely, we show in Fig. 7(a) the scattering in the low-temperature state near zone center [ $Q=(3.9,0,0)$ ] and at the zone boundary [ $Q=(3,0,0)$ ] along the  $[1,0,0]$  direction; the scattering at 100 K and  $Q=(3.5,0,0)$  is shown to demonstrate the level of background scattering. As in Fig. 6 there is no variation of the energy dependence [i.e., of the power spectrum  $P(E;T)$ ] with  $Q$ ; however, there does appear to be a significant increase in the peak intensity of the scattering (near  $E=45$  meV) at the zone boundary along  $[1,0,0]$  which would reflect an increase in the static susceptibility  $\chi(Q)$ . However, some of this apparent increase is due to variation in the background scattering with  $Q$ . This is shown in Fig. 7(b), where we present results for the peak intensity, as measured at a fixed energy transfer  $E=45$  meV, as a function of  $Q$  along the  $[1,0,0]$  direction. At each  $Q$  we again subtract the high-temperature (background) scattering from the low-temperature data, and plot the resulting low-temperature magnetic scattering as open circles; the solid line is at least-square fit to the data points. The scattering increases by a factor of 1.37 from zone center [ $Q=(4,0,0)$ ] to zone boundary [ $Q=(3,0,0)$ ] of which a factor of 1.23 is due to the larger form factor  $f^2(Q)$  at the smaller  $Q$ . Hence, there may be a weak (10%) increase in  $\chi(Q)$  from zone center to zone boundary along  $[1,0,0]$ .

## DISCUSSION

The degree to which  $\chi(Q)$  and  $P(E)$  depend on  $Q$  is a measure of the static and dynamic spatial correlations of the spin fluctuations. A  $Q$ -dependence characteristic of antiferromagnetic correlations has been observed in several heavy fermion compounds that are close to the trivalent limit and that have small (1–10 K) values for the characteristic (Kondo) temperature  $T_K$ .<sup>9</sup> For mixed-valent compounds with large  $T_K$ , most experimental studies of  $\chi''(Q;E)$  have been performed in polycrystals (e.g., Ref. 7), where the  $Q$  dependence cannot be determined. Theoretical studies of the Anderson lattice based on the random-phase approximation<sup>10</sup> or variational treatments<sup>11</sup> exhibit considerable  $Q$  dependence in both  $\chi(Q)$  and  $P(E)$ , arising from interband transitions across a gap that is predicted to arise from  $4f$ -conduction electron hybridization. For small hybridization, a peak in  $\chi(Q)$  is expected at the zone boundary; a zone boundary peak observed in TmSe has been interpreted in this manner.<sup>9</sup> Studies<sup>12</sup> of the one-dimensional Anderson lattice at half-filling (for which a ‘‘Kondo insulator’’ state occurs) show that the Ruderman-Kittel-Kasuya-Yoshida correlations observed for the symmetric (nearly integral valent) case disappear for the asymmetric mixed-valent case (where the  $4f$  level is near or at the Fermi level). An alternative assumption often made for mixed-valent compounds is that the spin fluctuations in mixed-valent compounds follow the predictions for a Kondo/Anderson impurity,<sup>13</sup> and hence should be highly local, with little  $Q$  dependence beyond that given by

the  $Q$  variation of the form factor. The ground-state line shape for  $P(E)$  predicted by Kuramoto and Müller-Hartmann<sup>14</sup> (KMH) using the Anderson model is shown in Fig. 4(b) as the filled symbols. The power function is very nearly Lorentzian: the solid line represents the form

$$P(E) \propto 1/\{(2\sin\alpha T_K)^2 + (E - 1.15T_K)^2\}, \quad (4)$$

where  $\sin\alpha = \sin[\pi n_f/(2J+1)] \approx 0.31$  for YbInCu<sub>4</sub> where  $J = \frac{7}{2}$  and the Yb  $4f$  hole occupation number (as determined<sup>1</sup> from  $L_3$  x-ray absorption) is  $n_f \approx 0.8$ .

For YbInCu<sub>4</sub>, a Lorentzian power spectrum gives an adequate description of the data, and within the uncertainties, there is no  $Q$  dependence of  $P(E)$ . Furthermore, while  $\chi(Q)$  appears to be larger at the zone boundary than at zone center, the effect is small (10%), so that the spin fluctuations are very nearly localized. We note, however, that the observed ratio of the linewidth to the peak position ( $\Gamma/E_0 = 12.3/40.2 = 0.31$ ) is somewhat smaller than that of Eq. (4) ( $2\sin/1.15 = 0.54$ ).

We also point out the consistency with the earlier work<sup>6</sup> performed in polycrystals. In that study, a time-of-flight spectrometer was employed; by summing the data for a number of detectors spanning a range of angles (and hence  $Q$ ) relatively good count rates and statistics were obtained. The correctness of this procedure is reinforced by our observation of the lack of significant  $Q$  dependence. The ground-state line shape was fit with a Lorentzian function centered at 40 meV, with a half-width of 18 meV; the ratio  $\Gamma/E_0 = 18/40 = 0.45$  is in better agreement with Eq. (4) than our result. However, this fit was obtained for a more limited range of energy transfer; the maximum energy transfer was 50 meV in that experiment compared to 65 meV in the present case. It would be worthwhile to repeat the time-of-flight study on polycrystals to higher-energy transfer to obtain a better determination of the line shape. In that study, the scattering in the high-temperature state was interpreted as arising from a pair of crystal-field levels; but since the linewidth of the scattering is as large as the excitation energy ( $\approx 2$  meV) we have chosen to treat it as a single broadened excitation, of Kondo type.

The relationship of our results to the static susceptibility is also in good agreement with the theory of a Kondo/Anderson impurity. The susceptibility predicted for a mixed-valent compound, using the Anderson model in the same approximation<sup>14</sup> as that leading to Fig. 4(b) and Eq. (4), satisfies  $\chi(0) = n_f C/T_K$ , where  $C$  is the Curie constant (for  $J = \frac{7}{2}$  Yb,  $C = 2.58$  emu K/mol). Given the peak position  $E_0^- = 40.2$  meV, then Eq. (4) gives  $T_K = 405$  K. For  $n_f = 0.8$ , the predicted susceptibility is  $\chi(0) = 0.0051$  emu/mol. For the data of Fig. 1 (after correction for a very small ‘‘Curie tail’’) the measured value is  $\chi(0) = 0.0056$  emu/mol. Similarly, for the high-temperature state,  $E_0^+ = 2.3$  meV, then KMH theory<sup>14</sup> for the case  $n_f = 1$  gives  $T_K = 25$  K; comparison<sup>4</sup> of the dc susceptibility data to the prediction of the  $J = \frac{7}{2}$  Kondo model gives  $T_K = 20$  K. Given the uncertainties in our data, this is excellent agreement.

## ACKNOWLEDGMENTS

Work at Irvine and Florida State was supported by the NSF under Grants Nos. DMR-9501528 and DMR-9501529, respectively. Work at Brookhaven was supported by the Division of Materials Research of the U.S. Department of Energy under Contract No. DE-AC02-76CH00016.

- <sup>1</sup>I. Felner *et al.*, Phys. Rev. B **35**, 6956 (1987).
- <sup>2</sup>K. Kojima *et al.*, J. Magn. Magn. Mater. **81**, 267 (1989); Phys. Soc. Jpn. **59**, 792 (1990).
- <sup>3</sup>D. C. Koskenmaki and K. A. Gschneidner, Jr., in *Handbook on the Physics and Chemistry of Rare Earths*, edited by K. A. Gschneidner, Jr. and L. Eyring (North-Holland, Amsterdam, 1978), Vol. 1, p. 337.
- <sup>4</sup>J. L. Sarrao *et al.*, Phys. Rev. B **54**, 12 014 (1996).
- <sup>5</sup>J. M. Lawrence *et al.*, Phys. Rev. B **54**, 6011 (1996).
- <sup>6</sup>A. Severing *et al.* Physica B **163**, 409 (1990).
- <sup>7</sup>E. Holland-Moritz *et al.*, Phys. Rev. B **25**, 7482 (1982).
- <sup>8</sup>C.-K. Loong *et al.*, Phys. Rev. B **35**, 3092 (1987).
- <sup>9</sup>G. Aeppli and C. Broholm, in *Handbook on the Physics and Chemistry of Rare Earths*, edited by K. A. Gschneidner and G. H. Lander (North-Holland, Amsterdam, 1994), Vol. 19.
- <sup>10</sup>P. S. Riseborough and D. L. Mills, Phys. Rev. B **21**, 5338 (1980).
- <sup>11</sup>B. H. Brandow, Phys. Rev. B **37**, 250 (1988).
- <sup>12</sup>M. Guerrero and C. C. Yu, Phys. Rev. B **51**, 10 301 (1995).
- <sup>13</sup>N. E. Bickers *et al.*, Phys. Rev. B **36**, 2036 (1987).
- <sup>14</sup>Y. Kuramoto and E. Müller-Hartmann, J. Magn. Magn. Mater. **52**, 122 (1985).